

**Nanocrystalline diamond AFM tips for chemical force spectroscopy: fabrication and photochemical functionalization†**Michael E. Drew,<sup>a</sup> Andrew R. Konicek,<sup>b</sup> Papot Jaroenapibal,<sup>c</sup> Robert W. Carpick<sup>\*d</sup> and Yoko Yamakoshi<sup>\*aef</sup>

Received 28th November 2011, Accepted 13th April 2012

DOI: 10.1039/c2jm16209a

The chemical modification of nanocrystalline diamond (NCD) atomic force microscope (AFM) tips was investigated and used for chemical force spectroscopy (CFS). In contrast to common chemical modification routes for gold or silicon AFM tips, this method creates stable C–C bonding to attach functional moieties to the NCD tip. There have been no previous studies reporting the chemical functionalization of NCD AFM tips. In this study, hydrogen-terminated NCDs (H-NCDs) were deposited on both silicon wafers and silicon AFM tips and subsequently subjected to a photochemical reaction with undecylenic acid (UA) to create UA attached to NCD surface (UA-NCD). The UA-NCD on wafers were used for surface analyses (water contact angle, attenuated total reflectance-Fourier transform infrared (ATR-FTIR), X-ray photoelectron spectroscopy (XPS), and near-edge X-ray absorption fine structure (NEXAFS) measurements) to confirm the chemical modification. The UA-NCD AFM tips were subjected to fluorescent labelling to confirm the existence of carboxylic acid on the tip and AFM adhesion measurements to assess their performance as a probe for the detection of chemical species on surfaces. These results indicate the promising ability of this method to serve as an ideal platform for CFS, which requires robust chemical functionalities on the AFM tip surfaces.

**1. Introduction**

There are increasing demands for new characterization methods with a high spatial resolution of the chemical functionality of surfaces. This is motivated by various factors, including the recent developments in nanolithography techniques that often involve multiple chemical functionalities on surfaces. Scanning tunnelling microscopy (STM) and atomic force microscopy (AFM) are the most effective surface analysis methods with atomic- or nanometre-scale spatial resolution. Standard AFM methods provide mainly topographical information of a sample, whereas lateral force and modulation methods provide insights into friction, structure, and mechanical properties. When

molecules with suitable functional groups are attached to AFM tips, it becomes possible to identify the chemical moiety of the surface *via* the intermolecular interaction between the molecules on the AFM tip and the surface. This technique is known as chemical force microscopy (CFM),<sup>1</sup> which provides adhesion force (pN level) and/or friction between the functional groups on an AFM tip and a sample surface. Such a chemical detection of the surface in nanometre-scale lateral resolution can be obtained only by CFM. However, a key obstacle for this technique is the stability of the organic molecules chemically bonded onto the AFM tip surface. Both the functionalized groups on the AFM tip surface and the tip itself must survive thousands of cycles in making contact, breaking contact, and sliding contact. In addition, the stress can be high in nanometre-scale contacts on the apex of AFM tips, leading to wear of the AFM tip material as well as contamination of its surface.<sup>2</sup> These stresses and repeated sliding can degrade the layer of molecules attached to both the surfaces of substrates and the tips.<sup>3</sup> Therefore, stable chemical functionalization methods for AFM tips are highly desirable.

Sulfur reactivity with gold surfaces (thiol, thioether, or disulfide) or silane chemistries with silicon are often used for the chemical functionalization of AFM surfaces.<sup>4</sup> Although these reactions are routinely used due to their high efficiency, these covalent bonds (*i.e.*, S–Au, or Si–O) are at risk of cleavage, thus limiting the lifetime of functionalized AFM tips. To address this important limitation of chemically modified AFM tips, in our previous studies, we functionalized Au-coated AFM tips by forming multiple S–Au bonds by the reaction of thiol or disulfide

<sup>a</sup>Department of Chemistry, University of Pennsylvania, 231 South 34<sup>th</sup> Street, Philadelphia, PA 19104-6323, USA<sup>b</sup>Department of Physics and Astronomy, University of Pennsylvania, 209 South 33<sup>rd</sup> Street, Philadelphia, PA 19104-6396, USA<sup>c</sup>Department of Material Science and Engineering, University of Pennsylvania, 3231 Walnut Street, PA 19104-6272, USA<sup>d</sup>Department of Mechanical Engineering and Applied Mechanics, University of Pennsylvania, 220 South 33<sup>rd</sup> Street, Philadelphia, PA 19104-6315, USA. E-mail: carpick@seas.upenn.edu; Fax: +1 215 573 6334; Tel: +1 215 898 4608<sup>e</sup>Laboratorium für Organische Chemie, ETH-Zürich, Wolfgang-Pauli-Strasse 10, CH-8093 Zürich, Switzerland. E-mail: yamakoshi@org.chem.ethz.ch; Fax: +41 44 633 1235; Tel: +41 44 633 6420<sup>f</sup>PRESTO, Japan Science and Technology Agency, Japan

† Electronic supplementary information (ESI) available. See DOI: 10.1039/c2jm16209a

with the gold surface. This was accomplished by using a tripod scaffold, which successfully provided a robust, stable attachment of organic molecules to the AFM tip while maintaining the desired chemical functionality.<sup>5,6</sup> An additional benefit of this system was increased separation of functional groups on the AFM tip due to the wider tripod scaffold to provide better isolated tip-sample adhesion formation to give a higher probability of single molecular force measurements. However, the risks of oxidative bond cleavage in S–Au and of plastic deformation or delamination of a soft gold film remain due to high contact stresses during CFM measurements. In the present study, we aim to develop a more stable functionalization method by using a photochemical reaction on hydrogen-terminated nanocrystalline diamond (H-NCD). There have been no previous studies reporting the chemical functionalization of H-NCD AFM tips. This chemical functionalization should provide extremely robust attachment of the organic molecule onto the AFM tips by creating a C–C bond linkage, which is more stable than S–Au or Si–O bonds.

Nanocrystalline diamond (NCD) AFM tips have been known since the early 1990's.<sup>7</sup> NCD and/or ultrananocrystalline diamond (UNCD) films<sup>8,9</sup> are mechanically stable and provide high resistance to wear.<sup>2,9–11</sup> By the addition of molecules *via* C–C bonds, a stable chemical functionalization can be introduced on the NCD surface. Taken together with low friction and low adhesion of NCD itself, we thought that it is an ideal AFM tip material for technological applications such as CFM, video-rate AFM imaging,<sup>11</sup> and tip-based nanolithography,<sup>12</sup> which are strongly limited by wear and contamination of the AFM tip apex.<sup>2,13,14</sup> The biocompatibility of diamond is additionally advantageous for the analyses of biomolecules. Also, the H-NCD surface can be regenerated by a hydrogen termination process so that the tip can be re-used for other modifications with different functionalities.

The photochemical reaction of alkenes and H-NCD surfaces is now a commonly used method of diamond functionalization.<sup>15</sup> Similar to a H-terminated Si surface,<sup>16</sup> UV exposure (254 nm) of H-NCD surfaces in the presence of terminal olefin molecules, such as undecylenic acid (UA), leads to alkanes that are bound to the diamond surface through C–C bonds.<sup>17–19</sup> The reaction rate can be accelerated in the presence of electron-accepting groups such as CF<sub>3</sub> in the molecule.<sup>20</sup> Amine-terminated diamond surfaces have been produced in this manner.<sup>21</sup> Taken together with the beneficial properties of diamond-based AFM tips above, we investigated the details of the photochemical reaction of H-NCD on the AFM tip apex to add a specific chemical functionality.

Although the chemical functionalization of a H-NCD surface has been known for a decade, the process is not fully understood. In this study, we initially carried out H-NCD deposition onto silicon wafers by CVD and subsequent photoreaction with UA to produce a UA-NCD film under our own conditions. The prepared UA-NCD films were characterized to confirm the covalent UA attachment by water contact angle, attenuated total reflectance-Fourier transform infrared (ATR-FTIR) spectroscopy, X-ray photoelectron spectroscopy (XPS), and near-edge X-ray absorption fine structure (NEXAFS) spectroscopy measurements, which require a relatively large surface area. Simultaneously, deposition and chemical functionalization of the

H-NCD AFM tip (Fig. 1) were carried out under exactly the same conditions as above. Since the number of surface analysis techniques, that are available for the verification of chemical functionalization of H-NCD AFM tips, are limited due to the small area of the AFM tip apex, UA-NCD tips were subjected to fluorescent labelling and AFM force adhesion measurements with terminally functionalized self-assembled monolayer (SAM) surfaces to confirm the UA attachment.

## 2. Material and methods

### 2.1. Materials

All solvents used were HPLC grade from Fisher Scientific (Fairlawn, NJ, USA). Silicon wafers were purchased from El-Cat Inc. (Waldwick, NJ, USA) and cut into pieces by a diamond cutter prior to use. Silicon AFM probes (CSC 37 without Al backsiding, MikroMasch, San Jose, CA, USA) were coated with NCD. Undecylenic acid (UA) was obtained from Acros (Morris Plains, NJ, USA) and was used as received. 1-Ethyl-3-(3'-dimethylaminopropyl)carbodiimide hydrochloride (EDC) and *N*-hydroxysuccinimide (NHS) were obtained from Sigma-Aldrich (St Louis, MO, USA). Fluorescein cadaverine was obtained from Biotium Inc. (Hayward, CA, USA).

### 2.2. Diamond deposition and subsequent hydrogen termination on silicon wafers or silicon AFM tips

NCD was deposited onto both silicon wafers and silicon AFM tips in a hot filament chemical vapour deposition chamber (HFCVD 007 diamond reactor chamber, Blue Wave Semiconductors, Baltimore, MD, USA). Prior to the deposition, a nanodiamond slurry in DMSO (>98% purity, cubic phase, 4–5 nm primary particle size, 30 nm average agglomerate size, International Technology Center, Research Triangle Park, NC, USA) was used for the seeding of diamond on silicon substrates. The seeding solution was prepared by combining 1 mL of nanodiamond slurry in 30 mL of MeOH (HPLC grade, Fisher Scientific, Fair Lawn, NJ, USA) and sonicating for 10 min. Silicon substrates were then soaked in the seeding solution for 30 min and subsequently cleaned by sonication in MeOH for 10 min, and dried with a stream of N<sub>2</sub>. This procedure produced a uniform, dense layer of nanodiamond particles on the Si surface, which act as nucleation sites for diamond film growth.

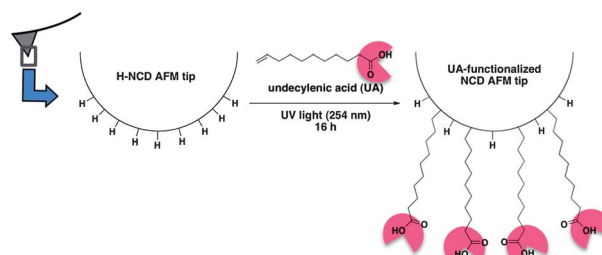


**Fig. 1** Photochemical functionalization of a H-terminated nanocrystalline diamond (H-NCD) AFM tip with a terminal alkene group (in this case, undecylenic acid, UA). Robust chemical functionalization of the AFM tip surface results through C–C covalent bonds.

Diamond deposition was carried out at 700 °C for one hour under an atmosphere of H<sub>2</sub>–CH<sub>4</sub> with a ratio of 96 : 4. Nano-diamond-seeded Si substrates were placed on the stage in the HFCVD chamber directly underneath the tungsten filaments (99.95% W wire, 0.5 mm diameter, Goodfellow Cambridge Ltd., Huntingdon, England). After a pressure of  $4 \times 10^{-3}$  Torr was reached, the chamber was filled with H<sub>2</sub> (90 sccm) and CH<sub>4</sub> (3.80 sccm) at a total pressure of 20–25 Torr. A substrate heater was ramped to 700 °C and held at that temperature for 60 minutes during NCD film growth. The pressure increased modestly as the chamber was heated and was maintained at 30 Torr during diamond deposition. The temperature of the W filament (~2000 °C) was sufficient to cleave the bonds in CH<sub>4</sub> and H<sub>2</sub>.

Directly after the diamond deposition, hydrogen termination (H-termination) treatment of surfaces was carried out by shutting off the CH<sub>4</sub> flow and filling the chamber with only H<sub>2</sub> (20 Torr, 700 °C) while keeping the filaments on. To ensure the successful creation of H-terminated surfaces after the filament power was shut off, the chamber pressure was kept at 20 Torr (of H<sub>2</sub>) until the substrate had cooled below 400 °C. NCD films deposited on silicon wafers were imaged by scanning electron microscopy (SEM) using a JEOL 7500F SEM (JEOL Ltd., Tokyo, JPN) and silicon AFM tips were imaged by transmission electron microscopy (TEM) using a JEOL 2010F TEM (JEOL).

### 2.3. Photochemical functionalization of H-NCD surface on silicon wafers or silicon AFM tips

Undecylenic acid (UA) was used for the photochemical functionalization of H-NCD surfaces. Identical procedures were used for H-NCD surfaces on both silicon wafers and silicon AFM tips. UA (mp 22–25 °C) was degassed by freeze/pump/thaw prior to use. The H-NCD silicon substrates were immersed in a quartz cell of neat UA which was filled with nitrogen gas and placed inside a photochemical reactor (Southern New England Ultraviolet Company, Middletown, CT, USA) equipped with five low-pressure 8 W Hg bulbs with a peak emission at a wavelength of 254 nm. The reaction was carried out for 16 hours and all the substrates were thoroughly washed by rinsing with dichloromethane, undergoing two cycles of sonication in dichloromethane for 10 min, subsequent sonication for 10 min in MeOH, and then dried with a stream of nitrogen.

### 2.4. Sessile drop contact angle measurements

A 3 µL drop of water (Millipore Milli-Q water, 18.2 MΩ, 0.2 µm filtered, Millipore Corp., Billerica, MA, USA) was placed on the sample surface. A CCD camera captured an image of the sample. The angle was measured using the Scion Image program (Scion Corp., Frederick, MD, USA).

### 2.5. Attenuated total reflectance-Fourier transform infrared (ATR-FTIR) analysis

ATR-FTIR spectroscopy was performed on a Nicolet 6700 spectrometer (Thermo Scientific, Waltham, MA, USA) with a Harrick grazing angle ATR (Harrick Scientific Products, Inc., Pleasantville, NY, USA) attachment. The angle of incidence was 65° and the MCT/A detector was cooled by liquid nitrogen. The Ge crystal was wiped with a methyl ethyl ketone-soaked cotton

swab and dried with a stream of nitrogen before and after each measurement. A total of 500 scans were taken for monolayer films on diamond with a resolution of 4 cm<sup>-1</sup>.

### 2.6. X-ray photoelectron spectroscopy (XPS) analysis

XPS spectra were obtained using a Perkin-Elmer 5400 ESCA spectrometer (PerkinElmer, Inc., Waltham, MA, USA) with a Mg Kα source without a monochromator. A 9° angle between the X-ray source and the sample normal was used with a 45° takeoff angle between the sample and the energy analyser.

### 2.7. Near-edge X-ray absorption fine structure (NEXAFS) analysis

NEXAFS spectra were obtained on beamline U7A at the National Synchrotron Light Source at Brookhaven National Laboratory (Upton, NY, USA). The incident beam angle was set to 90°, perpendicular to the surface for all spectra. The beamline uses a 600 line per mm grating with an exit slit set to 30 × 30 µm<sup>2</sup>. Carbon K-edge spectra were obtained from 275–355 eV and oxygen K-edge spectra were obtained from 520–580 eV. Partial electron yield spectra were obtained using a collector bias of –50 V and –300 V for the carbon and oxygen spectra, respectively. During each sample measurement, the measured photocurrent of an 85% transmissive gold mesh located upstream from the sample was collected. Normalization was performed by first dividing the raw spectra and photocurrent spectra to be unity in the pre-edge region, and then taking the ratio of the raw spectrum divided by the photocurrent spectrum. The spectra were further adjusted by subtracting the intensity of the pre-edge (first 5 eV of each spectrum) to zero. A single crystal of freshly H-terminated boron-doped diamond was measured as a standard. It had minimal π-bonded carbon at 285.0 eV and typical diamond features after 289 eV from the σ-bonded carbon in the sample. The C K-edge spectra had the energy axis shifted using a known feature in a simultaneously measured carbon spectrum.

### 2.8. Fluorescent labeling of AFM tips

After UA-functionalization, the UA-NCD tips were immersed in a solution of 1-ethyl-3-(3'-dimethylaminopropyl) carbodiimide hydrochloride (EDC, 200 mM) and N-hydroxysuccinimide (NHS, 250 mM) in PBS(–) for 24 h. The tips were rinsed with PBS(–) (pH = 7.4) and immersed in a  $1 \times 10^{-4}$  M solution of fluorescein cadaverine in PBS(–) for 1 h. The tips were washed with PBS(–) again and then sonicated in Millipore water for 10 min and washed and sonicated in acetone for 10 min. As a control, intact H-NCD tips (without UA functionalization) were treated under the same conditions. The tips were imaged by a fluorescent microscope (Olympus BX-51, Olympus Co., Tokyo, JPN) with a 75 W xenon bulb using the 10×, 20×, 50×, and 100× objectives. Images were collected with an Olympus digital camera.

### 2.9. Self-assembled monolayer (SAM) preparation on gold

Hydrogen flame-annealed gold surfaces (gold on mica, Agilent Technologies, Inc., Santa Clara, CA, USA) were immersed in a 1.0 mM ethanol solution of dodecane thiol (DDT,

Sigma-Aldrich) to produce the hydrophobic DDT-Au surface or in a 1.0 mM ethanol solution of 11-mercaptopundecanoic acid (MUA) to produce the hydrophilic MUA-Au surface. All ethanol solutions were degassed by freeze/pump/thaw before use. After 18 h of immersing in each solution, the gold substrates were washed exhaustively with ethanol to remove physically adsorbed molecules. The surfaces were used immediately after washing.

### 2.10. AFM adhesion force measurements

Adhesion measurements were performed on a Pico Plus 5500 AFM (Agilent Technologies, Inc.) in ethanol using a fluid cell. Ethanol was filtered (0.2  $\mu\text{m}$  PTFE filter, Millipore Corp.) before use. Force–distance curves were obtained with an approach rate of 100  $\text{nm s}^{-1}$ . The cantilever with the lowest spring constant on the chip was used in all measurements. The spring constant for each was calibrated by the Sader method<sup>22</sup> to be between 0.3 and 0.5  $\text{N m}^{-1}$ . Measurements were made for 20 force–distance curves at 10 different areas (200 total measurements) on each surface (DDT-Au or MUA-Au) using the identical tip before (H-NCD tip) and after (UA-NCD tip) the UA functionalization.

## 3. Results and discussion

### 3.1. Deposition and H-termination of the NCD onto the silicon substrates

SEM images of cleaved cross-sections showed that the H-NCD film deposited on Si wafers had a thickness of approximately 280 nm (Fig. S1b in the ESI†). The film thickness varied with the position of the sample relative to the W filaments. According to AFM measurements, the H-NCD surface had a root mean square (RMS) roughness of 12 nm over a scan size of 1  $\mu\text{m}^2$  (Fig. S2 in the ESI†). The water contact angle of the H-NCD surface was  $85 \pm 1^\circ$ , similar to the values reported for other H-NCD surfaces.<sup>23</sup>

A TEM image of a typical NCD AFM tip (Fig. 2) showed that the silicon tip was uniformly coated with a polycrystalline NCD layer with grain sizes of approximately 10–20 nm and a thickness of approximately 100 nm. Measured electron diffraction (Fig. 2, inset) patterns were consistent with the polycrystalline NCD structure reported.<sup>24,25</sup> The NCD-coated tip had a relatively large

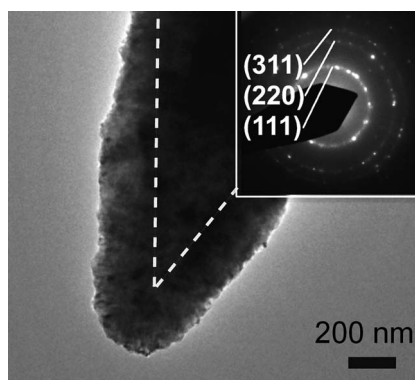


**Fig. 2** TEM image of a H-NCD-coated AFM tip. Dotted line shows the original silicon tip. Inset: electron diffraction pattern of the NCD-coated tip confirming the polycrystalline diamond structure.

radius of curvature (*ca.* 150 nm) compared to the original silicon AFM tip (dotted line in Fig. 2), but was usable for AFM study. These TEM images confirmed the presence of a uniform NCD film that completely covered the silicon tip and showed that the tip was suitable for photochemical functionalization.

### 3.2. Photochemical functionalization of H-NCD-coated silicon wafers

H-NCD films deposited on Si wafers were chemically treated under the identical conditions to those for the tips for the complementary surface characterization. The photochemical reactions of H-NCD surfaces were carried out by a neat reaction with liquid UA under UV light (254 nm). The resulting surfaces showed a lower water contact angle value ( $50 \pm 3^\circ$ ) than the initial H-NCD surfaces ( $85 \pm 1^\circ$ ), which we attribute to the attachment of carboxylic acid moieties on the surface. This value was higher than the reported values ( $<15^\circ$ ) for self-assembled monolayers (SAMs) of 11-mercaptopundecanoic acid ( $\text{HOOC}(\text{CH}_2)_{10}\text{SH}$ , MUA) on a Au (111) surface<sup>26</sup> that form well-packed SAM systems. This suggests that the density of  $-\text{COOH}$  groups on the UA-NCD films was less than that of Ba MUA SAM on gold. Moreover, the roughness of the NCD surface could inhibit the close packing of the UA layer, rendering it more disordered and providing a less hydrophilic surface. The latter effect was reported for alkylsilanes deposited on rough films consisting of silica nanoparticles.<sup>27</sup>

In the ATR-FTIR spectrum of an UA-NCD film (Fig. 3a), the methylene symmetric and antisymmetric stretches were observed at 2852 and 2926  $\text{cm}^{-1}$  with peak widths of 17 and 27  $\text{cm}^{-1}$ , respectively, confirming the attachment of UA to the H-NCD surface. The values were comparable to those of MUA SAMs on Au(111). The carbonyl stretch at 1709  $\text{cm}^{-1}$  agreed with the IR transmission spectrum of UA itself (Fig. 3b) and with previously

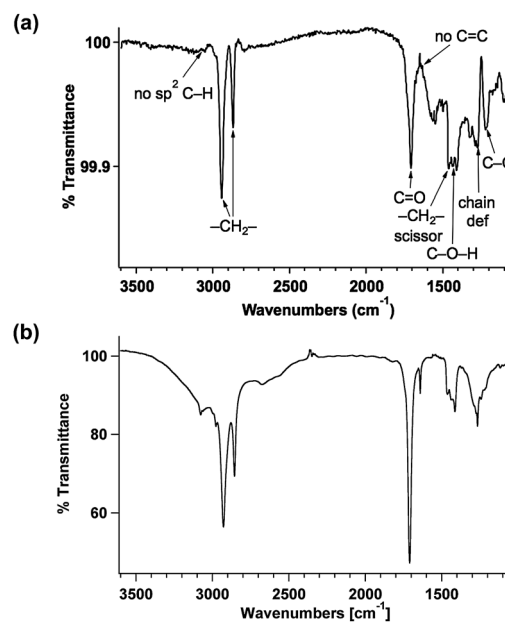


**Fig. 3** (a) ATR-FTIR spectrum of the UA-NCD surface (H-NCD was used as a background). (b) Transmission FTIR spectrum of a thin film of UA on a NaCl plate.

reported spectra of UA on silicon.<sup>28</sup> There was no shift in the carbonyl stretch and no observation of  $sp^2$  C–H stretches, indicating that the UA was attached to the NCD film by the reaction of the alkene and H-NCD and in the desired orientation with the functional group (COOH) furthest from the surface substrate. The absorption at  $1431\text{ cm}^{-1}$  was assigned to the C–O–H stretch.<sup>29</sup> The peak at  $1467\text{ cm}^{-1}$  was attributed to the  $-\text{CH}_2-$  scissor deformation and the peaks from  $1275\text{--}1330\text{ cm}^{-1}$  to alkyl chain wags and twists of UA. Additionally, the absorption at  $1215\text{ cm}^{-1}$  was assigned to the C–O stretch in the carboxylic acid.<sup>30</sup>

The XPS spectra (Fig. 4) showed reasonable results for chemical attachment of UA. Peak areas of UA-NCD revealed that the relative atomic percentages of near-surface carbon decreased from 84 at% to 77 at% while oxygen increased from 16 at% to 23 at% in comparison to H-NCD. High-resolution XPS spectra of UA-NCD revealed that the O 1s peak was relatively asymmetric and intense compared to H-NCD (Fig. 4c). The C 1s signal was more asymmetric with additional peaks at 286.7 eV and 289.1 eV (Fig. 4b), as expected for carboxylic acid groups. The presence of oxygen on the H-NCD surface prior to UA functionalization was speculated to be caused by adsorbed water and adventitious hydrocarbon contamination, which both result from exposure to laboratory air prior to XPS measurements.

NEXAFS analysis of the surfaces (Fig. 5) also supports the successful H- and UA-termination processes. The C *K*-edge spectra of H-NCD and UA-NCD samples were similar overall (Fig. 5a). The small peak at 285.0 eV indicates minimal  $sp^2$ -hybridized carbon, which is attributed to NCD grain boundaries. The edge jump at  $\sim 289.0$  eV and dip due to the second bandgap of diamond at 302.0 eV are unique characteristics of high quality diamond.<sup>9</sup> The two spectra differed between 286.0 and 289.0 eV, where C–H (287.5 eV), C–O (288.5 eV), and C=O (286–289 eV, depending on the molecular geometry) intensities occur.<sup>31</sup> While the individual peaks were too small and closely spaced to be resolved, increased relative intensity for the UA-NCD sample in this range is consistent with surface attachment of alkyl carboxylic acids. Moreover, increases in O *K*-edge intensity at

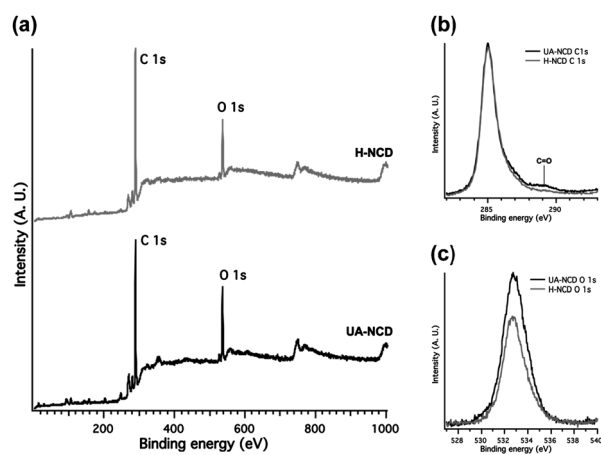


**Fig. 4** X-ray photoelectron spectra of H-NCD and UA-NCD surfaces. (a) Survey spectra of H-NCD and UA-NCD samples, (b) C 1s spectra of H-NCD and UA-NCD samples, and (c) O 1s spectra of H-NCD and UA-NCD samples.

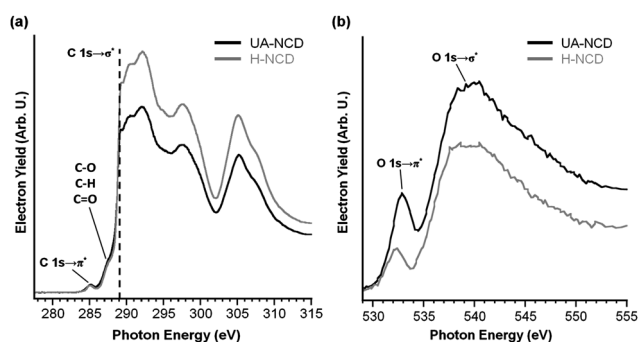


**Fig. 5** NEXAFS partial electron yield spectra of H-NCD and UA-functionalized nanocrystalline diamond (UA-NCD). (a) C *K*-edge spectra and (b) O *K*-edge spectra.

532.9 eV and 539.7 eV (Fig. 5b) for  $\pi$ - and  $\sigma$ -bonded oxygen, respectively, also indicated the presence of UA. The NEXAFS spectra were normalized such that differences in chemical content affect the total intensity. The UA-NCD oxygen signal is higher, showing the chemical modification by addition of oxygen species. The UA-NCD carbon signal is lower for UA-NCD as there is now a lower density organic layer, which contains hydrogen, covering the diamond surface. Consistent with the XPS measurements, some oxygen was present prior to UA functionalization. Regardless, significantly more oxygen was observed on the UA-NCD surface as expected.

### 3.3. Photochemical functionalization of H-NCD-coated silicon AFM tips

UA-NCD AFM tip preparation was carried out under identical conditions to those of the UA-NCD surface preparation described in Section 3.2. Prepared UA-NCD AFM tips were evaluated by fluorescent labelling, which involved activation of the carboxylic acids on the AFM tip to *N*-hydroxysuccinimide esters and the subsequent treatment with fluorescein cadaverine (scheme in Fig. 6). As a control, non-functionalized H-NCD AFM tips were treated under the same conditions. By fluorescent microscopy analysis, UA-NCD AFM tips showed significant fluorescent intensity (Fig. 6a), while the control showed no fluorescence on the cantilever (Fig. 6c). Focusing on the tip apex,  $\sim 20\ \mu\text{m}$  above the plane of the cantilever, fluorescent intensity was observed on the tip apex down to the lateral spatial resolution limit of this microscope ( $\sim 1\ \mu\text{m}$ ) (Fig. 6b) which provided strong evidence for the successful functionalization of H-NCD AFM tips with UA.

### 3.4. AFM adhesion measurements by a chemically functionalized NCD tip

The UA-NCD and H-NCD tips were used for AFM adhesion force measurements against MUA (with terminal  $-\text{COOH}$ ) or DDT (with terminal alkane) SAM adsorbed onto a gold surface substrate. All measurements were performed in ethanol to reduce capillary force effects. Two hundred adhesion measurements of a H-NCD or UA-NCD tip against a MUA or DDT sample produced the four histograms shown in Fig. 7. The control H-NCD tip had adhesion forces (mean  $\pm$  margin of error  $E$  for

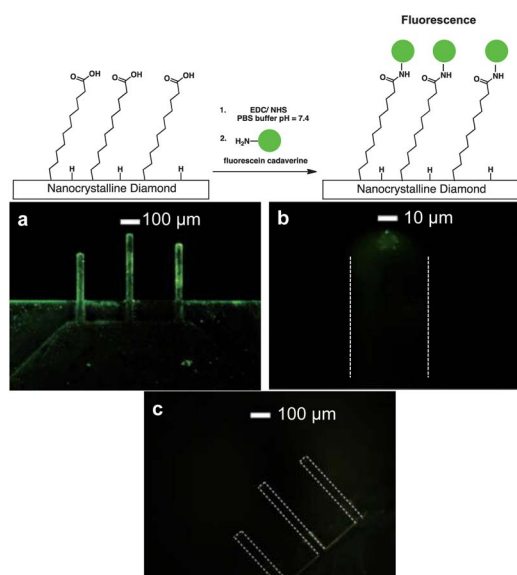


**Fig. 6** Fluorescence optical microscope images of AFM cantilevers after fluorescent labeling: (a) fluorescence image of UA-NCD cantilever, (b) fluorescence image of UA-NCD cantilever focusing on the tip apex which is slightly above the cantilever plane, and (c) fluorescent image of an intact H-NCD cantilever.

a 95% confidence interval) of  $0.36 \pm 0.02$  nN on DDT-Au and  $0.21 \pm 0.02$  nN on MUA-Au (Fig. 7a and b). In contrast, the UA-NCD tip had adhesion forces of  $0.35 \pm 0.05$  nN on the DDT-Au and  $1.27 \pm 0.07$  nN on MUA-Au (Fig. 7c and d). The

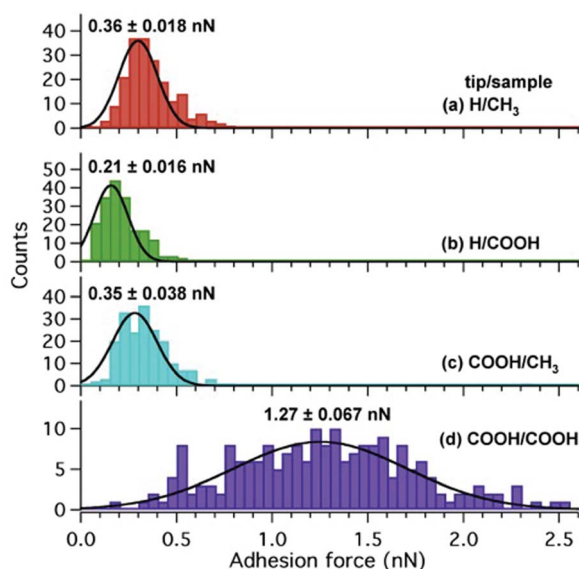


**Fig. 7** Histogram of adhesion forces with either an H-NCD or UA-NCD AFM tip on functionalized gold SAM surfaces. (a) H-NCD tip on a DDT-Au surface. (b) H-NCD tip on a MUA-Au surface. (c) UA-NCD tip on a DDT-Au surface. (d) UA-NCD tip on a MUA-Au surface. Numbers are mean margin of error  $E$  for a 95% confidence interval. Standard deviations are (a) 0.127, (b) 0.108, (c) 0.271, and (d) 0.475. Based on the Student's  $t$ -tests, difference between (a) and (b), (a) and (d), (b) and (c), (b) and (d), and (c) and (d) were significant, but the difference between (a) and (c) was not significant.

largest adhesion occurred between the UA-NCD tip and the MUA-Au sample (Fig. 7d) was due to the hydrogen bonding between the carboxylic acids on the tip and on the sample. This increased adhesion confirmed the successful functionalization of the diamond tip with carboxylic acid groups. As a hydrophobic entity, the H-NCD tip only experiences van der Waals attraction to each sample and, as expected, these forces are slightly greater on the hydrophobic sample (Fig. 7a) than on the hydrophilic one (Fig. 7b).<sup>1</sup> Similarly, the UA-NCD tip exhibited low adhesion with the DDT-Au surface (Fig. 7c).

While one might expect that the hydrophilic–hydrophobic pairings should give similar adhesion values regardless of which groups are on the tip or substrate, we observed lower adhesion between the H-NCD tip and the MUA-Au sample (Fig. 7b) compared to that between the UA-NCD tip and the DDT-Au sample (Fig. 7c). This subtle but statistically significant effect may be due to tip curvature and roughness, since roughness disrupts the packing of the UA chains such that they do not uniformly display their carboxylic acid groups, as reported for alkylsilanes on rough films composed of silica nanoparticles.<sup>26</sup> While the density and conformation of the UA molecules on the tip remain to be quantified, the adhesion measurements clearly support the claim that the tips have been successfully functionalized with UA.

#### 4. Conclusions

We have documented the first successful fabrication of chemically functionalized NCD AFM tips. H-NCD films on silicon wafers and silicon AFM tips were prepared by HFCVD and then subjected to photochemical reaction with UA to create carboxylic acid-terminated NCD (UA-NCD) surfaces. The water contact angle, as well as ATR-FTIR, XPS, and NEXAFS spectroscopy measurements all give evidence of the successful functionalization of NCD films with UA. UA-NCD AFM tips showed enhanced fluorescence when subjected to carboxylic acid-selective labelling conditions. They exhibited substantially greater adhesion with acid-terminated SAMs than with alkane-terminated SAMs, and also exhibited greater adhesion than that measured between H-NCD AFM tips and acid- or alkane-terminated surfaces. Taken together, these data confirm the successful molecular functionalization of diamond AFM probes.

Chemically modified NCD AFM tips have important potential for use in advanced scanning probe-based applications due to their robustness and biocompatibility originating from the stable modification *via* C–C bonds. Ongoing work focusing on preparing more densely packed monolayers of UA on H-NCD AFM tips, achieving smaller tip radii, and attaching other synthetic molecules to NCD tips for biomolecular recognition studies will be reported in the near future.

#### Acknowledgements

The authors thank Dr D. S. Grierson at the University of Wisconsin-Madison for acquiring the XPS spectra. The authors thank Mr T. D. B. Jacobs and Mr S. Ghassemi in the Department of Mechanical Engineering and Applied Mechanics at the University of Pennsylvania for their assistance with TEM images and for acquiring SEM images. The authors thank Prof. A. B.

Smith III in the Department of Chemistry at the University of Pennsylvania for the generous use of his photoreactor. The authors thank Prof. C. Kagan in the Department of Materials Science and Engineering at the University of Pennsylvania for the use of the ATR-FTIR spectrometer. This research was partially supported by the Nano/Bio Interface Center through the National Science Foundation NSEC (DMR08-32802) and JST PRESTO program from the Japan Science and Technology Agency. The use of University of Pennsylvania Nano/Bio Interface Center instrumentation is acknowledged. The use of Penn Regional nanotechnology Facility of the University of Pennsylvania is acknowledged. The use of the National Synchrotron Light Source in the Brookhaven National Laboratory was supported by the U.S. Department of Energy, Office of Science, and Office of Basic Energy Sciences, under contract no. DE-AC02-98CH10886.

## References

- 1 C. D. Frisbie, A. Noy, C. M. Lieber, L. F. Rozsnyai and M. S. Wrighton, *Abstracts of Papers of the American Chemical Society*, 1994, **208**, 221–COLL.
- 2 K. T. Turner, J. Liu, D. S. Grierson, N. Moldovan, J. Notbohm, S. Li, P. Jaroenapibal, S. D. O'Connor, A. V. Sumant, N. Neelakantan, J. A. Carlisle and R. W. Carpick, *Small*, 2010, **6**, 1140–1149.
- 3 J. D. Kiely and J. E. Houston, *Langmuir*, 1999, **15**, 4513–4519.
- 4 H. J. Gruber, A. Ebner, L. Wildling, R. Zhu, C. Rankl, T. Haselgrubler and P. Hinterdorfer, *STM and AFM Studies on (Bio)Molecular Systems: Unravelling the Nanoworld*, 2008, vol. 285, pp. 29–76.
- 5 M. E. Drew, A. Chworos, E. Oroudjev, H. Hansma and Y. Yamakoshi, *Langmuir*, 2010, **26**, 7117–7125.
- 6 D. Takamatsu, K. Fukui, S. Aroua and Y. Yamakoshi, *Org. Biomol. Chem.*, 2010, **8**, 3655–3664.
- 7 G. J. Germann, G. M. McClelland, Y. Mitsuda, M. Buck and H. Seki, *Rev. Sci. Instrum.*, 1992, **63**, 4053–4055.
- 8 A. Erdemir, C. Bindal, G. R. Fenske, C. Zuiker, A. R. Krauss and D. M. Gruen, *Diamond Relat. Mater.*, 1996, **5**, 923–931.
- 9 A. R. Konicek, D. S. Grierson, P. U. P. A. Gilbert, W. G. Sawyer, A. V. Sumant and R. W. Carpick, *Phys. Rev. Lett.*, 2008, **100**, 235502.
- 10 W. P. King, P. C. Fletcher, J. R. Felts, Z. T. Dai, T. D. Jacobs, H. J. Zeng, W. Lee, P. E. Sheehan, J. A. Carlisle and R. W. Carpick, *ACS Nano*, 2010, **4**, 3338–3344.
- 11 L. M. Picco, L. Bozec, A. Ulcinas, D. J. Engledew, M. Antognozzi, M. A. Horton and M. J. Miles, *Nanotechnology*, 2007, **18**, 044030.
- 12 R. D. Piner, J. Zhu, F. Xu, S. H. Hong and C. A. Mirkin, *Science*, 1999, **283**, 661–663.
- 13 C. M. Su, L. Huang, K. Kjoller and K. Babcock, *Ultramicroscopy*, 2003, **97**, 135–144.
- 14 H. Bhaskaran, B. Gotsmann, A. Sebastian, U. Drechsler, M. A. Lantz, M. Despont, P. Jaroenapibal, R. W. Carpick, Y. Chen and K. Sridharan, *Nat. Nanotechnol.*, 2010, **5**, 181–185.
- 15 T. Strother, T. Knickerbocker, J. N. Russell, J. E. Butler, L. M. Smith and R. J. Hamers, *Langmuir*, 2002, **18**, 968–971.
- 16 T. Strother, W. Cai, X. S. Zhao, R. J. Hamers and L. M. Smith, *J. Am. Chem. Soc.*, 2000, **122**, 1205–1209.
- 17 Y. L. Zhong, K. F. Chong, P. W. May, Z. K. Chen and K. P. Loh, *Langmuir*, 2007, **23**, 5824–5830.
- 18 B. M. Nichols, J. E. Butler, J. N. Russell and R. J. Hamers, *J. Phys. Chem. B*, 2005, **109**, 20938–20947.
- 19 S. Wenmackers, S. D. Pop, K. Roodenko, V. Vermeeren, O. A. Williams, M. Daenen, O. Douheret, J. D'Haen, A. Hardy, M. K. Van Bael, K. Hinrichs, C. Cobet, M. vandeVen, M. Ameloot, K. Haenen, L. Michiels, N. Esser and P. Wagner, *Langmuir*, 2008, **24**, 7269–7277.
- 20 P. E. Colavita, J. A. Streifer, B. Sun, X. Y. Wang, P. Warf and R. J. Hamers, *J. Phys. Chem. C*, 2008, **112**, 5102–5112.
- 21 A. Hartl, E. Schmich, J. A. Garrido, J. Hernando, S. C. R. Catharino, S. Walter, P. Feulner, A. Kromka, D. Steinmuller and M. Stutzmann, *Nat. Mater.*, 2004, **3**, 736–742.
- 22 J. E. Sader, J. W. M. Chon and P. Mulvaney, *Rev. Sci. Instrum.*, 1999, **70**, 3967–3969.
- 23 J. M. Garguilo, B. A. Davis, M. Buddie, F. A. M. Kock and R. J. Nemanich, *Diamond Relat. Mater.*, 2004, **13**, 595–599.
- 24 L. C. Nistor, J. VanLanduyt, V. G. Ralchenko, E. D. Obraztsova and A. A. Smolin, *Diamond Relat. Mater.*, 1997, **6**, 159–168.
- 25 T. Lin, G. Y. Yu, A. T. S. Wee, Z. X. Shen and K. P. Loh, *Appl. Phys. Lett.*, 2000, **77**, 2692–2694.
- 26 C. E. D. Chidsey and D. N. Loiacono, *Langmuir*, 1990, **6**, 682–691.
- 27 J. D. Batteas, R. L. Jones and N. C. Pearsall, *J. Phys. Chem. C*, 2009, **113**, 4507–4514.
- 28 R. Voicu, R. Boukherroub, V. Bartzoka, T. Ward, J. T. C. Wojtyk and D. D. M. Wayner, *Langmuir*, 2004, **20**, 11713–11720.
- 29 R. Arnold, W. Azzam, A. Terfort and C. Woll, *Langmuir*, 2002, **18**, 3980–3992.
- 30 R. G. Nuzzo, L. H. Dubois and D. L. Allara, *J. Am. Chem. Soc.*, 1990, **112**, 558–569.
- 31 J. Stöhr, in *NEXAFS Spectroscopy*, Springer-Verlag, New York, USA, 1992.